ROBOTIC CONTROL

A memristor-based hybrid analog-digital computing platform for mobile robotics

Buyun Chen[1]*, Hao Yang[1]*, Boxiang Song[1], Deming Meng[1], Xiaodong Yan[1], Yuanrui Li[1], Yunxiang Wang[1], Pan Hu[1], Tse-Hsien Ou[1], Mark Barnell[2], Qing Wu[2], Han Wang[1], Wei Wu[1]†

Algorithms for mobile robotic systems are generally implemented on purely digital computing platforms. Developing alternative computational platforms may lead to more energy-efficient and responsive mobile robotics. Here, we report a hybrid analog-digital computing platform enabled by memristors on a mobile inverted pendulum robot. Our mobile robotic system can tune the conductance states of memristors adaptively using a model-free optimization method to achieve optimal control performance. We implement sensor fusion and the motion control algorithms on our hybrid analog-digital computing platform and demonstrate more than one order of magnitude enhancement of speed and energy efficiency over traditional digital platforms.

INTRODUCTION

Improvements in computing power efficiency are diminishing over time as performance gains due to complementary metal-oxide semiconductor scaling near their end (*1*, *2*). This issue affects the power requirements of large data centers and could limit the performance of mobile robotic systems with perception and actuation (*2*, *3*). Requirements for computing power increase commensurate with the complexity of mobile robotic systems (*3*). The growing demand of the computing power and the saturation of Moore's law limit the development of mobile robotic systems with more functions and higher degrees of freedom (DOFs). Therefore, the development of an alternative computing platform with higher speed and power efficiency for mobile robotics would be ideal.

The control of the human body is enabled by the highly sophisticated, ultralow-power computational capability of the human brain. The human brain (*4*) consists of the cerebrum, the cerebellum, and the brainstem. The cerebrum is a major part of the brain in charge of vision, hearing, and thinking, whereas the cerebellum plays an important role in motion control. Through this cooperation of the cerebrum and the cerebellum, the human brain can conduct multiple tasks simultaneously with extremely low power consumption. Inspired by this, we developed a hybrid analog-digital computation platform, in which the digital component runs the high-level algorithm, whereas the analog component is responsible for sensor fusion and motion control. Forty years ago, a similar approach was proposed (*5*, *6*). Unfortunately, this approach has never been adopted widely, owing to technological limitations [lack of electronically reconfigurable devices and silicon integrated circuits (IC)–compatible analog devices to implement such systems efficiently].

With the development of memristors, it is now possible to implement such a system efficiently. The memristor is a two-terminal IC-compatible analog device, which can be programmed precisely to different conductance states (*7*–*9*). The tunable conductance states of the memristor enable the computation in-memory architecture, which is considered a promising candidate to address the von Neumann bottleneck. The memristor is ideal for the analog computing because it offers excellent scalability, a broad range of IV linearity, and nonvolatility. In addition, space-saving and cost-effectiveness make the memristor a greater candidate to develop electronically reconfigurable analog circuits than other analog computing devices (*10*) (see table S1). A mobile robot, as a real-time control system, can benefit substantially from the memristor-based hybrid computing platform with higher speed and power efficiency. Both the sensor fusion algorithm and motion control algorithm can be expressed as linear equations, which can be performed by analog circuits with memristors. The digital platform, however, consumes more time and energy because it needs to store and compute the information separately. Moreover, the memristor-based analog component can operate independently without using the computing resources from the digital component. This parallel computing architecture is essential for further increasing the DOFs of mobile robotic systems. So far, the memristor-based hybrid computing platform has enhanced the computing efficiency in supervised, unsupervised, and reinforcement learning (*11*–*15*). However, demonstrations of memristor-based hybrid computing platforms in robotic systems are rare.

In this study, we demonstrate a one-DOF low-latency self-adaptive mobile robotic system using our proposed memristor-based hybrid analog-digital computing platform. The sensor fusion algorithm (a single Kalman filter) and the motion control algorithm, a single proportional-derivative (PD) controller, are implemented using a customized analog circuit with two memristors to control the motion of the robot. The reconfigurability of the memristor is used to enable the robot to adapt to a changing environment. Because the computation speed of the analog component is much faster than that of the digital component, the latency of Kalman filter and motion control in the robot is substantially reduced. The computation cycle time of the hybrid platform is minimized to 6 μs, which includes the time to read the processed analog signal (4 μs) and the time to transfer the data to the digital motor driver (2 μs). Also, because the Kalman filter and motion control are both implemented on the analog component, the signal can be directly read and processed from sensors to motion controller without quantization error. There is no need for analog-to-digital converters (ADCs) and digital-to-analog converters (DACs), thus substantially reducing the power, space, and cost while improving its performance. In addition, the Kalman filter

[1]Ming Hsieh Department of Electrical and Computer Engineering, University of Southern California, Los Angeles, CA 90089, USA. [2]Air Force Research Laboratory, Information Directorate, Rome, NY 13441, USA.
*These authors contributed equally to this work.
†Corresponding author. Email: wu.w@usc.edu

algorithm and the motion control algorithm are separated from the high-level algorithms in the hybrid platform, thus reducing the computation load of the digital component. We show that the mobile robotic system using hybrid computing platform with higher speed-energy efficiency performs better (shorter settling time, faster response, and better stability) than the same robot with the traditional digital platform (see note S1 for details).

RESULTS

Analog-digital hybrid platform enabled by memristor

A mobile inverted pendulum (*16*) was chosen to demonstrate our memristor-based analog-digital hybrid platform. It is a mobile robotic system with many applications (*17*). However, the high latency and large power consumption in the conventional digital platform limit the performance of the mobile inverted pendulum (*18*). Our proposed hybrid analog-digital computing platform can address the above challenges.

Figure 1 (A and B) shows our proposed hybrid analog-digital computing platform. The digital component implements high-level algorithms (e.g., perception algorithm and decision-making algorithm), which serves as the "cerebrum" of the robot brain. Meanwhile, memristor-based analog components implement sensing and motion control algorithm, which act as the "cerebellum" of the robot brain. More specifically, a continuous-time Kalman filter using a memristor-based analog component was implemented, and it is responsible for the sensor fusion (Fig. 1A). The motion control function (Fig. 1A) is realized by a PD controller (*16*) using the memristor-based analog component.

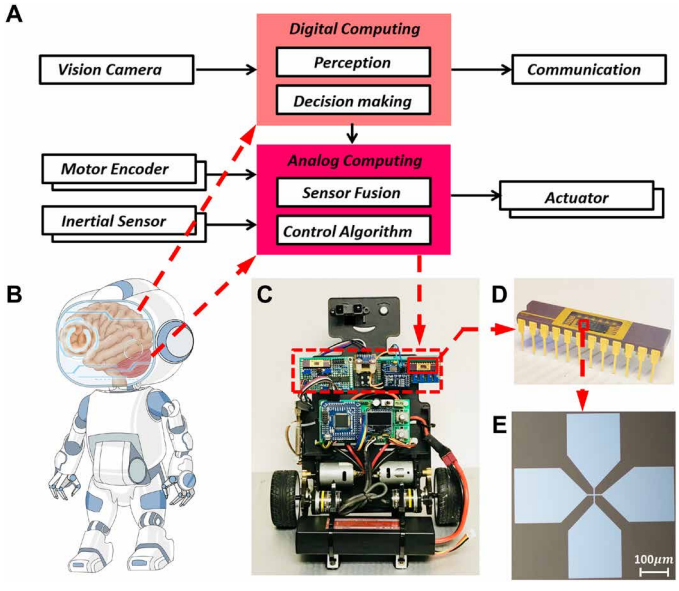

Fig. 1. The memristor-based hybrid analog-digital computing platform. (**A**) Schematic illustration of hybrid analog-digital computing platform. (**B**) Schematic representation of the biological inspiration from the brain structure. In the hybrid analog-digital computing platform, the analog component acts as the cerebellum that controls the motion of the robot, whereas the digital component acts as the cerebrum running the high-level algorithms. (**C**) Image of the mobile robotic system (i.e., the mobile inverted pendulum) in this work. (**D**) Image of the memristors packaged on the chip carrier. (**E**) Optical microscope image of the fabricated Pt/Al_2O_3/Ta/Pt cross-point memristor; scale bar, 100 μm.

Pt/Al_2O_3/Ta/Pt memristors were used for our proposed hybrid analog-digital computing platform (*19*). The typical IV curve (Fig. 2A) of our memristor demonstrates an excellent IV linearity, which is ideal for the analog computing. The inset of Fig. 2A shows the four-layer structure of the Pt/Al_2O_3/Ta/Pt memristor. The device can be tuned to multiple conductance states using both DC voltage sweep (Fig. 2B) and voltage pulses (Fig. 2C) with different compliance current. The compliance current is controlled using the serial transistor (R6015KNX, Rohm Semiconductor) with different voltages applied (Fig. 2, D to F). The difference of the device response between the potentiation and the depression is caused by different tuning protocols (see fig. S1 for details). Using a feedback detection method, the Pt/Al_2O_3/Ta/Pt memristor can be precisely tuned with an SD of 9 μs (fig. S2). As a result, the Pt/Al_2O_3/Ta/Pt memristor can provide 141 (more than 7 bits) conductance states ranging from 450 to 3000 μs. Moreover, small device-to-device variation (fig. S3, A and B), high endurance (fig. S3C), and long retention time (fig. S3D) are demonstrated in Pt/Al_2O_3/Ta/Pt memristors. These characteristics guarantee the reliability of the device, thus the hybrid analog-digital platform. Figure 1 (C to E) shows the home-built mobile inverted pendulum, the memristor packaged on the chip carrier, and the optical microscope image of the Pt/Al_2O_3/Ta/Pt cross-point memristor, respectively. Details are introduced in the following sections.

Hardware acceleration of Kalman filter

Precisely detecting the angle of the system is necessary for controlling a mobile inverted pendulum successfully. In the mobile inverted pendulum (Fig. 1C), an accelerometer and a gyroscope are typically used to detect the angle and angular velocity signals of the mobile inverted pendulum, respectively. The accelerometer measures the angle of the system by measuring the acceleration along the vertical axis. However, the white noise in the sensor measured signal is inevitable, which causes instability in the mobile inverted pendulum.

The Kalman filter (*20*–*23*) is the most commonly used method to perform signal preprocessing and to filter the white noise. Traditionally, the analog signal is detected by the sensor, converted to the digital signal via ADCs, and then transported to the digital processor through a communication bus. After that, the signal is processed using a discrete-time Kalman filter on the digital platform. All the above procedures consume a substantial amount of power and cause high latency (*24*). To solve this problem, a memristor-based analog circuit is prototyped to realize the continuous-time Kalman filter, as shown in Fig. 3 (A and B). In the continuous-time analog Kalman filter, the measured signal is processed physically without conversion to the digital domain, thereby minimizing both the latency and the quantization error. Therefore, the Kalman filter can be accelerated notably using hardware.

In the continuous-time Kalman filter (*20*, *25*), the system model and measure model of the angle measurement can be defined as

$$\begin{bmatrix} \dot{\theta}(t) \\ \dot{bias}(t) \end{bmatrix} = \begin{bmatrix} 0 & -1 \\ 0 & 0 \end{bmatrix} \begin{bmatrix} \theta(t) \\ bias(t) \end{bmatrix} + \begin{bmatrix} 1 \\ 0 \end{bmatrix} \omega_{mea}(t) + w(t) \quad (1)$$

$$\theta_{mea}(t) = [1\ 0] \begin{bmatrix} \theta(t) \\ bias(t) \end{bmatrix} + v(t) \quad (2)$$

where $\theta(t)$ is the ideal angle of the system, $bias(t)$ is the bias error of the angular velocity, $\omega_{mea}(t)$ is the measurement of the angular

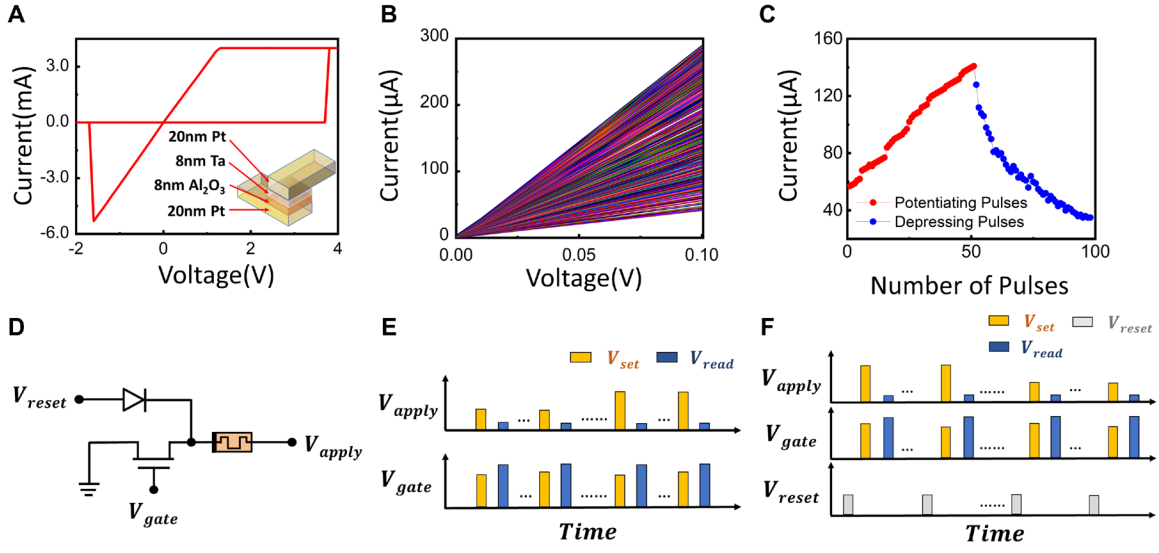

Fig. 2. Schematic and electrical characteristics of the Pt/Al_2O_3/Ta/Pt memristor. (**A**) I-V characteristics of the Pt/Al_2O_3/Ta/Pt memristor (plot in linear scale) from 5 μm by 5 μm Pt/Al_2O_3/Ta/Pt cross-point memristors. This memristor has excellent I-V linearity and large on/off ratio. The inset of Fig. 1A shows the structure of the Pt/Al_2O_3/Ta/Pt cross-point memristor. Twenty-nanometer Pt was deposited as top and bottom electrode. Eight-nanometer Ta and 8-nm Al_2O_3 work as active layer and switching layer, respectively. (**B**) The memristor can be precisely set to different conductance states using DC sweep voltages with different compliance currents. The I-V characteristics for a Pt/Al_2O_3/Ta/Pt memristor with different conductance states are shown. (**C**) The conductance state response under potentiating pulses (red) and depressing pulses (blue). (**D**) Circuit schematic diagram for pulse tuning. The bottom electrode of the memristor is connected to the drain of the transistor to build a one transistor and one resistor structure. Different voltage pulses applied on the pulse tuning circuit are V_{apply}, V_{gate}, and V_{reset}. The voltage on the top electrode of the memristor (V_{apply}) and the reset voltage (V_{reset}) are used to control the set or the reset process of the memristor, and the compliance current is controlled by the gate voltage (V_{gate}). Waveforms of potentiating pulses (**E**) and depressing pulses (**F**). During the potentiating process, the memristor is only programmed by set pulses (V_{set}). Both reset pulses (V_{reset}) and set pulses (V_{set}) are used in the depressing process. The conductance state of the memristor is measured without being changed via reading pulses (V_{read}). Details including pulse width and amplitudes are given in the Supplementary Materials (fig. S1).

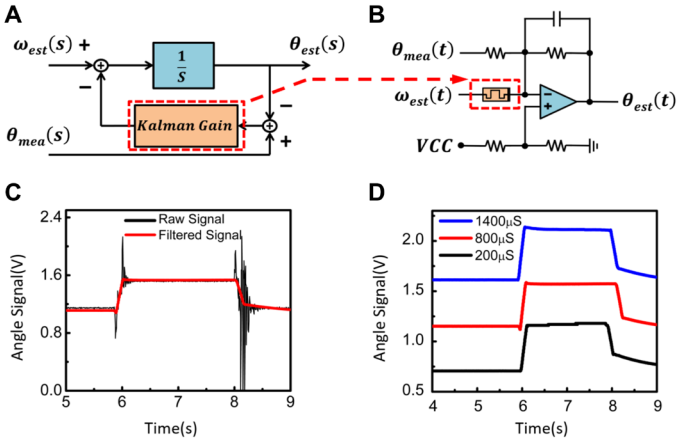

Fig. 3. Hardware acceleration of continuous-time analog Kalman filter. (**A**) Block diagram of angle signal estimation with continuous-time analog Kalman filter. The estimated angle signal [$\theta_{est}(s)$] can be obtained after the Kalman filter with input signals from both the gyroscope [$\omega_{est}(s)$] and the accelerometer [$\theta_{mea}(s)$]. The complex frequency in Laplace transform is denoted *S*. (**B**) Circuit schematic diagram of the hardware implementation of the continuous-time analog Kalman filter, where the Kalman gain (K_1) is implemented using a memristor. The 5-V voltage is denoted *VCC*. (**C**) Measured raw data of the angle signal (black curve) and the filtered data (red curve) by the continuous-time analog Kalman filter. The test was performed on a rotating robotic arm (fig. S5). (**D**) Estimated angle signals with different Kalman gains (different conductance states of memristor). An overlarge conductance state causes overshoot response (blue curve), whereas an insufficient conductance state causes overdamped response (black curve). The optimized conductance state of the memristor (red curve) was chosen for the continuous-time analog Kalman filter using the binary search method.

velocity, $w(t)$ is the white noise of the system model, $\theta_{mea}(t)$ is the measurement signal of the accelerometer, and $v(t)$ is the white noise of the measure model. In addition, $w(t)$ and $v(t)$ are mutually uncorrelated.

Using Eqs. 1 and 2, the estimate update equation can be expressed as

$$\begin{bmatrix} \dot{\theta}_{est}(t) \\ \dot{bias}_{est}(t) \end{bmatrix} = \begin{bmatrix} 0 & -1 \\ 0 & 0 \end{bmatrix} \begin{bmatrix} \theta_{est}(t) \\ bias_{est}(t) \end{bmatrix} + \begin{bmatrix} 1 \\ 0 \end{bmatrix} \omega_{mea}(t) + \begin{bmatrix} K_1 \\ K_2 \end{bmatrix} [\theta_{mea}(t) - \theta_{est}(t)] \quad (3)$$

where the vector $[K_1 \quad K_2]^T$ is the Kalman gain (*20*) of the estimate update equation. Equation 3 can be simplified further. On the basis of the readout signal of the sensor where the white noise is negligible, it is reasonable to assume that the bias error from the gyroscope is a constant, and thus the Kalman gain K_2 of the estimate bias is expected to be 0. In addition, the $bias_{est}(t)$ can be measured directly from the voltage output of the gyroscope and then the angular velocity can be reconstructed, as shown in Eq. 4

$$\omega_{est}(t) = \omega_{mea}(t) - bias_{est}(t) \quad (4)$$

After the above simplifications, Eq. 3 can be expressed as

$$\dot{\theta}_{est}(t) = \omega_{est}(t) + K_1 [\theta_{mea}(t) - \theta_{est}(t)] \quad (5)$$

It has been proved that the Kalman gain will converge to a constant after several iterations (*20*). Because the Kalman gain is implemented using a memristor, the memristor only needs to be programmed once when environment changes dramatically. The nonvolatile nature of memristor ensures that the Kalman gain K_1

is still reserved even though the mobile robotic system is shut off. The transfer function block diagram (Fig. 3A) shows Eq. 5 in the frequency domain. Figure 3B shows the circuit schematic diagram of the continuous-time analog Kalman filter. The details of the parameters are given in the Supplementary Materials (fig. S4, A and B).

To test and optimize the continuous-time analog Kalman filter, we built a robotic arm, which can swing between 45° and 135° horizontally (fig. S5). The sensor was mounted on the robotic arm to measure various angles. The black curve in Fig. 3C shows that the raw measured angle signal is very noisy. Because the noise can cause instability in the mobile inverted pendulum, the raw measured signal cannot be directly used to compute the motion control signal. For comparison, the signal filtered by our continuous-time analog Kalman filter (Fig. 3C, red curve) eliminates the noise and reconstructs the ideal signal, which demonstrates the feasibility of our proposed analog Kalman filter.

As mentioned above, the Kalman gain is determined by the conductance of the memristor. Therefore, the dynamic response of the Kalman filter circuit depends on the memristor conductance state. An excessively large conductance can cause overshoot in the filter response, whereas a small conductance can lead to overdamping. The response of the Kalman filter circuit is also affected by sensors and environment. For example, even with the same model (see Methods for details) and the same Kalman gain, different gyroscopes may cause different filter responses (fig. S6A). Overshoot and overdamping can also occur when the temperature changes (fig. S6B). Therefore, to achieve the best performance of the Kalman filter, the conductance of the memristor needs to be optimized before using it in the robot. A binary search method is adopted in this process. In the first step, this method chooses two conductance values (a high value and a low value) in the memristor to generate both the overshoot and overdamped responses, respectively. Then, the conductance value will be reprogrammed to a new value between the two initial values. If there is an overdamped initial response in the circuit, the search interval for the subsequent conductance value can be narrowed down to the upper half of the range between the initial values; otherwise, it can be narrowed to the lower half of this range. The performance of the Kalman filter can be optimized within eight iterations using this method because the total number of states of the memristor is around 7 bits. Once the optimal conductance state (Fig. 3D, red curve) of the memristor is chosen, there should be no overshoot (Fig. 3D, blue curve) or overdamped (Fig. 3D, black curve) response in the filtered signal. Compared with the discrete-time Kalman filter implemented on the digital platform, the continuous-time analog Kalman filter substantially accelerates the sensor fusion process and reduces the computing load of the digital component. The details can be found in note S1.

Hardware acceleration of adaptive PD controller

Except for filtering the measured angle signal, the controller is also important toward successfully balancing the mobile inverted pendulum. Controlling a mobile inverted pendulum is not an easy task, because the nonlinearity of the dynamical system is inevitable and difficult to analyze. Generally, this nonlinearity of the mobile inverted pendulum mainly comes from the high latency due to the long cycle time of the computation. Many nonlinear controllers have been proposed to mitigate the nonlinear effect, such as neural network controllers and fuzzy logic controllers (*26*–*28*). However, these controllers have not reduced the cycle time. The nonlinearity of the system still exists, thus limiting the upper bound of the robotic system performance. In this study, we proposed and demonstrated an adaptive PD controller using a memristor-based hybrid analog-digital computing platform, which notably reduces the computation cycle time, thus fundamentally solving the nonlinearity problem.

The dynamic model of an ideal mobile inverted pendulum is very similar to the cart-pole scenario (*29*). The body of the inverted pendulum is free to rotate because of the gravitational force. To balance the body of the inverted pendulum, the inertial force generated by the acceleration of the inverted pendulum needs to be equal to the force because of the gravity. The linear dynamic model can be roughly defined as

$$L\frac{d^2\theta(t)}{dt^2} = g\theta(t) - u(t) + Lw(t) \tag{6}$$

where $u(t)$ is the acceleration of the motion, $w(t)$ is the disturbance of the environment, and L is the length of the robot. Because the time constant of the motor is much larger than the cycle time, the torque of the motor (i.e., acceleration of motion) can be considered as being proportional to the voltage applied on the motor. Therefore, the function of the controller is to create proper movement of the robot to balance itself. According to previous research (*16*, *30*), $u(t)$ is defined as

$$u(t) = K_p\theta(t) + K_d\frac{d\theta(t)}{dt} \tag{7}$$

where K_p is the proportional term and K_d is the derivative term of the controller. By combining Eqs. 6 and 7, the mobile inverted pendulum can be considered as a damped harmonic oscillator, and it can be modeled as

$$\frac{d^2\theta(t)}{dt^2} + \frac{K_d}{L}\frac{d\theta(t)}{dt} + \frac{K_p - g}{L}\theta(t) = w(t) \tag{8}$$

The schematic representation and the block diagram of the mobile inverted pendulum with the PD controller are shown in Fig. 4 (A and B, respectively). In the PD controller, K_p and K_d can be considered as the spring constant of an elastic spring and the damping coefficient of a damper, respectively. In the experiment, a single memristor is used to implement the damping ratio K_d/K_p of the controller. The schematic diagram of the circuit is shown in Fig. 4C. The damping ratio is determined by the conductance state of the memristor. The details of the parameters of the circuit are given in the Supplementary Materials (fig. S4, C and D). Figure 4D provides an overview of the hardware structure of the control system of the mobile inverted pendulum. The impulse responses (Fig. 4E) of the mobile inverted pendulum are measured in the experiment. The result indicates that as the conductance value of the memristor (damping ratio) increases, the oscillation of the mobile inverted pendulum decreases as expected.

The conductance states of memristors need to be optimized for the mobile inverted pendulum in different scenarios. In other words, the mobile inverted pendulum is expected to work in different unknown situations, where the motion acceleration $u(t)$, depending on both the interaction with the environment and the load on the robot, will be unpredictable. Therefore, the parameters must be optimized in different cases. The random search algorithm is adopted

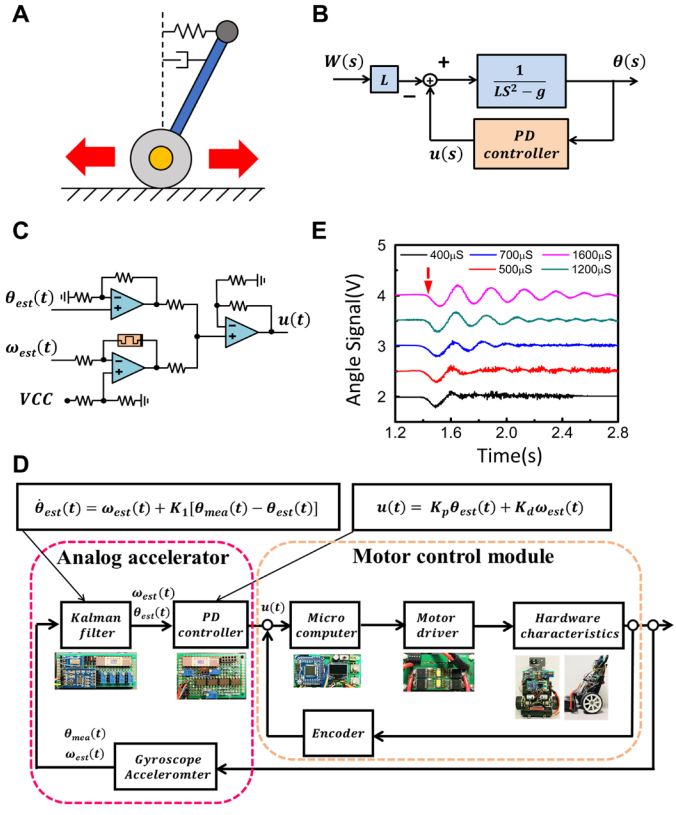

Fig. 4. Hardware acceleration of the analog PD controller. (**A**) Schematic of the mobile inverted pendulum with the PD controller, which can be considered a simple damped harmonic oscillator. (**B**) Block diagram of the transfer function of the mobile inverted pendulum with a PD controller, where θ(*t*) is the angle of the mobile inverted pendulum, *u*(*s*) is the acceleration of the motion, *W*(*s*) is the disturbance of the environment, *L* is the length of the robot, and *g* is the gravity of Earth. The complex frequency in Laplace transform is denoted *S*. (**C**) Circuit schematic diagram of the hardware implementation of the analog PD controller, where the damping ratio (K_d/K_p) was implemented using a memristor. The acceleration of the motion [*u*(*t*)] was directly obtained from the analog PD controller given the estimated angle [$\theta_{est}(t)$] and angular velocity signals [$\omega_{est}(t)$]. The 5-V voltage is denoted *VCC*. (**D**) Hardware structure of the control system of the mobile inverted pendulum. (**E**) Experimental data of several impulse responses of the mobile inverted pendulum at different conductance states of the memristor. The red arrow indicates the disturbance.

in the robot (*31*). This is a model-free method, which can optimize the parameters of the system without knowing the exact physical model of the robot. This optimization problem can be expressed as

$$minimize\, E_{e_t,\omega}\left[\Sigma_{t=1}^{T} C_t(x_t, u_t)\right] \quad (9)$$

$$s.\,t.\quad x_{t+1} = f_t(x_t, u_t, e_t) \text{ and } u_t = \pi(\tau_t; K + \omega)$$

where the cost function used to describe the system vibration can be written as

$$C(K) = \Sigma_{t=0}^{n} (\theta_K(t) - \theta_0)^2 \quad (10)$$

where θ_0 is 0 in the system. However, it is impossible to get all the physical parameters accurately in reality; thus, the traditional optimization method using gradient descent cannot be applied. To know the tuning direction of parameters, the gradient $G(\omega, K)$ of the cost function $C(K)$ is tested from the system.

$$G(\omega, K) = \frac{1}{m}\Sigma_{i=1}^{m} \frac{C(K + \sigma\omega_i) - C(K - \sigma\omega_i)}{2\sigma}\omega_i \quad (11)$$

The flowchart in Fig. 5A schematically illustrates the adaptive learning process. During each learning epoch, the control performances of the certain memristor conductance value both with and without introducing a small perturbation (adding a 200-ohm resistor in serial) are tested. Then, the cost function can be calculated and thus determines the direction of optimization. Both the simulated and experimental data (Fig. 5B) show that the cost function converges after 15 learning epochs. This indicates the feasibility of our optimization method. Here, the Runge-Kutta method (*32*) is used to simulate the dynamic model of the mobile inverted pendulum with nonlinearity, including both the latency and the finite acceleration effect. The details of the experimental data can be found in the Supplementary Materials (fig. S7).

The memristor-based hybrid platform yields much better performance in speed and energy efficiency compared with the traditional digital platforms (see note S1). Therefore, the control performance of the mobile inverted pendulum is substantially improved using the hybrid platform with much lower latency (see fig. S8 for details). As indicated in Fig. 5C, the settling time of the mobile inverted pendulum with our hybrid analog-digital computing platform is about 1 s. Using the traditional digital platform (see fig. S9 for details), the mobile inverted pendulum is still not perfectly stabilized even after more than 3 s. In addition, the mobile inverted pendulum using our hybrid platform has a much faster response (Fig. 5D) than the one using a traditional digital platform. The comparison of the impulse responses of the mobile inverted pendulum using different platforms can be found in the Supplementary Materials (movie S1). The cycle time of the mobile inverted pendulum using our hybrid analog-digital computing platform (6 μs) is notably smaller than the one with a traditional digital platform (3034 μs), so the mobile inverted pendulum using hybrid computing platform can achieve much better control performance.

DISCUSSION

A mobile inverted pendulum robot with a hybrid analog-digital computing platform using memristors is successfully demonstrated in this work. All the circuit components were built using conventional electronics devices except for the memristors. The reconfigurability of the memristors enabled the mobile robot to adapt to the environment through analog computing. The memristor-based analog components were designed as a bio-inspired implementation of the cerebellum in the robot brain, whereas the digital component implementing high-level algorithms served as the cerebrum of the robot brain. The memristor-based analog component can operate independently without consuming the computing power from the digital component. Through this cooperation of the cerebrum and the cerebellum, the robot can conduct multiple tasks simultaneously with a much shorter latency and lower power consumption. In addition, the power consumption of the hybrid computing platform can be further reduced by integrating all the circuit components on a single chip (*33*). A further potential benefit of applying the memristor-based hybrid platform in the robotics application is the

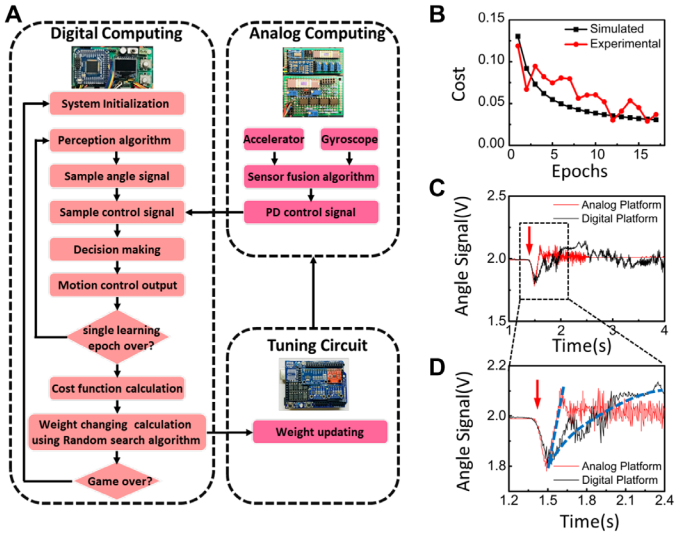

Fig. 5. The adaptive learning process on the hybrid computing platform and the optimal control performance. (**A**) Flowchart of the random search optimization algorithm implementation on the memristor-based hybrid analog-digital computing platform. During each learning epoch, the control performances of certain memristor conductance states with and without small perturbation (adding a 200-ohm resistor) were tested. Then, the cost function and its gradient were calculated from the angle signal data accordingly. After that, the weight of the memristor was updated toward minimizing the cost function. (**B**) Simulated (black curve) and experimental (red curve) data of the adaptive learning process. (**C**) The settling time of the mobile inverted pendulum with the hybrid platform (~1 s) is much shorter than the one with the digital platform (more than 3 s). The red arrow indicates the disturbance. (**D**) The difference of the slope (blue dashed line) of the angle signal shows that the mobile robotic system using the hybrid platform has a faster response than the one using the digital platform. The red arrow indicates the disturbance.

prevention of the aging effect of memristors (*34*). The memristor in the Kalman filter does not require frequent calibration, and the memristor in the PD controller only needs to be initialized when the environment changes dramatically. Because the memristors are not frequently reprogrammed, the lifetime of the memristor in the robotic application will be longer than that of the memristor used in other applications, which require constant reprograming (*34*).

In conclusion, this work proposes and demonstrates a one-DOF mobile robot using a hybrid analog-digital computing platform based on memristors, with an equivalent 141-level precision and excellent I-V linearity. Both the Kalman filter algorithm and the control algorithm, the two main functions of the cerebellum, were implemented and accelerated using this hybrid platform. We leveraged the reconfigurability of memristors to demonstrate an adaptive learning approach for the robot. Compared with the mobile inverted pendulum using conventional digital computing platform, the robot with hybrid computing platform not only achieved better stability and faster response but also yielded one order of magnitude of enhancement in speed and energy efficiency (see note S1). With the enhancement in performance, our hybrid computing platform has the potential to improve the robustness and the performance of the mobile robotic systems with higher DOFs. We also anticipate that the memristor-based hybrid analog-digital computing platform can be used for a broad spectrum of applications in the future, such as Internet of Things and edge computing applications.

MATERIALS AND METHODS

Device fabrication

The devices are Pt/Al_2O_3/Ta/Pt memristors. First, SiO_2 film (150 nm) was grown on a Si wafer via thermal oxidation using furnace (Thermco Products Corporation, MB71). Then, a lift-off layer (Shipley Microposit LOL 2000) and a photoresist layer (AZ MiR 701) were spin-coated onto the substrate. Photolithography (54.3 mJ/cm^2) was performed with a customized photomask. After postbake (110°C for 1 min) procedure and development (AZ 300 MIF Developer), an adhesion layer (2-nm Ti) and bottom electrode (20-nm Pt) were deposited onto the substrate using e-beam evaporation (Temescal BJD 1800 E-Beam Evaporator). The liftoff process was then conducted using the acetone solution with ultrasound vibration. After that, an 8-nm Al_2O_3 blanket layer was deposited using a plasma enhanced atomic layer deposition (ALD) process (Oxford PlasmaPro 100). Last, an active layer (8-nm Ta) and top electrode (20-nm Pt) were defined using a second photolithography, e-beam evaporation, and lift-off process using the same recipes above.

Device characterization

Both DC electrical characterizations and multilevel conductance states measurement were carried out with a Keithley 4200 semiconductor characterization system. The system can be programmed to meet the requirements of different experiments. During the measurement, the top and bottom electrodes were directly connected to the probes. A microscope can help correctly align the device to a certain position. The voltage sweep mode has multiple sweeping functions with high-precision measurement, which offers accurate measurement of the electrical property of the device. In addition, the module can be programmed to measure multiple times automatically. By controlling the compliance currents from 20 to 200 μA, the memristor can be set precisely to the target state.

Robotic system setup

The mobile inverted pendulum was built on the custom-designed mechanical platforms. For the mobile inverted pendulum using our memristor-based hybrid analog-digital computing platform, an accelerometer (model: NXP MMA7361) and a gyroscope (model: SMAKN ENC-03RC) were used to detect the angle and angular velocity signals of the robot. Then, the signals were processed physically using memristor-based analog circuits (the details of the circuits are discussed in the previous sections). The main board and the motor control module were also custom-designed on two printed circuit boards, respectively. Both the circuit layout and the printed circuit boards are shown in the Supplementary Materials. The firmware that supports the mobile robotic system is available at https://github.com/buyunchen/mobile-inverted-pendulum.

SUPPLEMENTARY MATERIALS

robotics.sciencemag.org/cgi/content/full/5/47/eabb6938/DC1

Fig. S1. Waveforms of potentiating pulses and depressing pulses.
Fig. S2. The precise tuning ability of the memristor.
Fig. S3. Device electrical characterization.
Fig. S4. The detail parameters of the analog Kalman filter and analog controller.
Fig. S5. The robotic arm for testing the Kalman filter.
Fig. S6. Performances of the analog Kalman filter under different cases.
Fig. S7. The experimental data during the self-learning process.
Fig. S8. Hardware design for the hybrid robotic system.
Fig. S9. Hardware design for the digital robotic system.
Table S1. The comparison of different electronically reconfigurable analog circuits.
Table S2. The comparison of speed and power efficiency on different platforms.

Note S1. Performance analysis of the memristor-based hybrid analog-digital computing platform in comparison with the conventional digital computing platform.
File S1. Circuit diagram of the hybrid robotic system.
File S2. Circuit diagram of the digital robotic system.
Movie S1. The comparison of control performance on different platforms.
References (*35*–*40*)

REFERENCES AND NOTES

1. M. M. Waldrop, The chips are down for Moore's law. *Nature* **530**, 144–147 (2016).
2. R. S. Williams, What's next? [The end of Moore's law]. *Comput. Sci. Eng.* **19**, 7–13 (2017).
3. T. Matsui, H. Hirukawa, Y. Ishikawa, N. Yamasaki, S. Kagami, F. Kanehiro, H. Saito, T. Inamura, Distributed real-time processing for humanoid robots, in *11th IEEE International Conference on Embedded and Real-Time Computing Systems and Applications (RTCSA'05)* (IEEE, 2005), pp. 205–210.
4. R. S. Frackowiak, *Human Brain Function* (Elsevier, 2004).
5. E. A. Devjanin, V. S. Gurfinkel, E. V. Gurfinkel, V. A. Kartashev, A. V. Lensky, A. Y. Shneider, L. G. Shtilman, The six-legged walking robot capable of terrain adaptation. *Mech. Mach. Theory* **18**, 257–260 (1983).
6. V. S. Gurfinkel, E. V. Gurfinkel, A. Y. Shneider, E. A. Devjanin, A. V. Lensky, L. G. Shtilman, Walking robot with supervisory control. *Mech. Mach. Theory* **16**, 31–36 (1981).
7. H.-S. P. Wong, H.-Y. Lee, S. Yu, Y.-S. Chen, Y. Wu, P.-S. Chen, B. Lee, F. T. Chen, M.-J. Tsai, Metal–oxide RRAM, in *Proceedings of the IEEE* (IEEE, 2012), vol. 100, pp. 1951–1970.
8. D. B. Strukov, G. S. Snider, D. R. Stewart, R. S. Williams, The missing memristor found. *Nature* **453**, 80, 83 (2008).
9. J. J. Yang, D. B. Strukov, D. R. Stewart, Memristive devices for computing. *Nat. Nanotechnol.* **8**, 13–24 (2013).
10. E. H. Lee, S. S. Wong, Analysis and design of a passive switched-capacitor matrix multiplier for approximate computing. *IEEE J. Solid State Circuits* **52**, 261–271 (2017).
11. S. H. Jo, T. Chang, I. Ebong, B. B. Bhadviya, P. Mazumder, W. Lu, Nanoscale memristor device as synapse in neuromorphic systems. *Nano Lett.* **10**, 1297–1301 (2010).
12. C. Li, Z. Wang, M. Rao, D. Belkin, W. Song, H. Jiang, P. Yan, Y. Li, P. Lin, M. Hu, N. Ge, J. P. Strachan, M. Barnell, Q. Wu, R. S. Williams, J. J. Yang, Q. Xia, Long short-term memory networks in memristor crossbar arrays. *Nat. Mach. Intell.* **1**, 49–57 (2019).
13. Z. Wang, S. Joshi, S. Savel'ev, W. Song, R. Midya, Y. Li, M. Rao, P. Yan, S. Asapu, Y. Zhuo, H. Jiang, P. Lin, C. Li, J. H. Yoon, N. K. Upadhyay, J. Zhang, M. Hu, J. P. Strachan, M. Barnell, Q. Wu, H. Wu, R. S. Williams, Q. Xia, J. J. Yang, Fully memristive neural networks for pattern classification with unsupervised learning. *Nat. Electron.* **1**, 137–145 (2018).
14. Z. Wang, C. Li, W. Song, M. Rao, D. Belkin, Y. Li, P. Yan, H. Jiang, P. Lin, M. Hu, J. P. Strachan, N. Ge, M. Barnell, Q. Wu, A. G. Barto, Q. Qiu, R. S. Williams, Q. Xia, J. J. Yang, Reinforcement learning with analogue memristor arrays. *Nat. Electron.* **2**, 115–124 (2019).
15. C. Li, M. Hu, Y. Li, H. Jiang, N. Ge, E. Montgomery, J. Zhang, W. Song, N. Dávila, C. E. Graves, Z. Li, J. P. Strachan, P. Lin, Z. Wang, M. Barnell, Q. Wu, R. S. Williams, J. J. Yang, Q. Xia, Analogue signal and image processing with large memristor crossbars. *Nat. Electron.* **1**, 52–59 (2017).
16. F. Grasser, A. D'arrigo, S. Colombi, A. C. Rufer, JOE: A mobile, inverted pendulum. *IEEE Trans. Ind. Electron.* **49**, 107–114 (2002).
17. M. Nikpour, L. Huang, A. M. Al-Jumaily, B. Lotfi, Stability control of mobile inverted pedulum through an added movale mechanism, in *2018 25th International Conference on Mechatronics and Machine Vision in Practice (M2VIP)* (IEEE, 2018), pp. 1–6.
18. C. B. Schindler, T. Watteyne, X. Vilajosana, K. S. Pister, Implementation and characterization of a multi-hop 6TiSCH network for experimental feedback control of an inverted pendulum, in *2017 15th International Symposium on Modeling and Optimization in Mobile, Ad Hoc, and Wireless Networks (WiOpt)* (IEEE, 2017), pp. 1–8.
19. H. Yang, B. Chen, B. Song, D. Meng, S. C. Tiwari, A. Krishnamoorthy, X. Yan, Z. Liu, Y. Wang, P. Hu, T.-H. Ou, P. Branicio, R. Kalia, A. Nakano, P. Vashishta, F. Liu, H. W. W. Wu, Memristive device characteristics engineering by controlling the crystallinity of switching layer material. *ACS Appl. Electron. Mater.* **2**, 1529–1537 (2020).
20. F. L. Lewis, L. Xie, D. Popa, *Optimal and Robust Estimation: With an Introduction to Stochastic Control Theory* (CRC Press, 2017).
21. R. E. Kalman, A new approach to linear filtering and prediction problems. *J. Basic Eng.* **82**, 35–45 (1960).
22. E. J. Lefferts, F. L. Markley, M. D. Shuster, Kalman filtering for spacecraft attitude estimation. *J. Guid. Control Dynam.* **5**, 417–429 (1982).
23. G. Hee Lee, F. Faundorfer, M. Pollefeys, Motion estimation for self-driving cars with a generalized camera, in *Proceedings of the IEEE Conference on Computer Vision and Pattern Recognition* (2013), pp. 2746–2753.
24. H. Hur, H.-S. Ahn, Discrete-time H_∞ filtering for mobile robot localization using wireless sensor network. *IEEE Sens. J.* **13**, 245–252 (2012).
25. B. Ristic, S. Arulampalam, N. Gordon, Beyond the Kalman filter. *IEEE Aeros. Electron. Syst. Magaz.* **19**, 37–38 (2004).
26. H. Lee, S. Jung, Balancing and navigation control of a mobile inverted pendulum robot using sensor fusion of low cost sensors. *Mechatronics* **22**, 95–105 (2012).
27. J. Seul, K. Sung Su, Control experiment of a wheel-driven mobile inverted pendulum using neural network. *IEEE Trans. Control Syst. Technol.* **16**, 297–303 (2008).
28. T. Abut, S. Soyguder, Real-time control and application with self-tuning PID-type fuzzy adaptive controller of an inverted pendulum. *Ind. Robot* **46**, 159–170 (2019).
29. W. Zhong, H. Rock, Energy and passivity based control of the double inverted pendulum on a cart, in *Proceedings of the 2001 IEEE International Conference on Control Applications (CCA'01)(Cat. No. 01CH37204)* (IEEE, 2001), pp. 896–901.
30. F. M. Atay, Balancing the inverted pendulum using position feedback. *Appl. Math. Lett.* **12**, 51–56 (1999).
31. D. C. Karnopp, Random search techniques for optimization problems. *Automatica* **1**, 111–121 (1963).
32. S. Gottlieb, C.-W. Shu, Total variation diminishing Runge-Kutta schemes. *Math. Comput. Am. Math. Soc.* **67**, 73–85 (1998).
33. T. Gokmen, Y. Vlasov, Acceleration of deep neural network training with resistive cross-point devices: Design considerations. *Front. Neurosci.* **10**, 333 (2016).
34. S. Zhang, G. L. Zhang, B. Li, H. H. Li, U. Schlichtmann, Aging-aware lifetime enhancement for memristor-based neuromorphic computing, in *2019 Design, Automation & Test in Europe Conference & Exhibition (DATE)* (IEEE, 2019), pp. 1751–1756.
35. C. N. Lau, D. R. Stewart, R. S. Williams, M. Bockrath, Direct observation of nanoscale switching centers in metal/molecule/metal structures. *Nano Lett.* **4**, 569–572 (2004).
36. G. Akgün, H. ul Hasan Khan, M. A. Elshimy, D. Göhringer, Dynamic tunable and reconfigurable hardware controller with EKF-based state reconstruction through FPGA-in the loop, in *2018 International Conference on ReConFigurable Computing and FPGAs (ReConFig)* (IEEE, 2018), pp. 1–8.
37. J. Ordóñez Cerezo, E. Castillo Morales, J. M. Cañas Plaza, Control system in open-source FPGA for a self-balancing robot. *Electronics* **8**, 198 (2019).
38. V. Šetka, R. Čečil, M. Schlegel, Triple inverted pendulum system implementation using a new ARM/FPGA control platform, in *2017 18th International Carpathian Control Conference (ICCC)* (IEEE, 2017), pp. 321–326.
39. S. Seok, A. Wang, M. Y. M. Chuah, D. J. Hyun, J. Lee, D. M. Otten, J. H. Lang, S. Kim, Design principles for energy-efficient legged locomotion and implementation on the MIT cheetah robot. *IEEE/ASME Transa. Mechatronics* **20**, 1117–1129 (2014).
40. S. Sarathy, M. M. Hibah, S. Anusooya, S. Kalaivani, Implementation of efficient self balancing robot, in *2018 International Conference on Recent Trends in Electrical, Control and Communication (RTECC)* (IEEE, 2018), pp. 65–70.

Acknowledgments: The fabrications were performed at the Keck Photonics Center at the University of Southern California. **Funding:** W.W. acknowledges the support from the US Air Force Research Laboratory (AFRL) (grant no. FA-8750-19-1-0503). Any opinions, findings, and conclusions or recommendations expressed in this material are those of the authors and do not necessarily reflect the views of AFRL or its contractors. H.W. acknowledges the support from the Army Research Office Young Investigator Program (grant no. W911NF1810268).
Author contributions: B.C. and H.Y. contributed equally to this study. B.C., H.Y., and W.W. designed the experiments. B.C., H.Y., B.S., and D.M. fabricated the devices. B.C., X.Y., and H.W. performed electrical measurements. B.C., H.Y., B.S., D.M., Y.L., Y.W., P.H., T.-H.O., M.B., Q.W., and W.W. performed the analyses. W.W. supervised the work. B.C, H.Y., H.W., and W.W. composed the manuscript. All authors reviewed and commented on the manuscript. **Competing interests:** The authors declare that they have no competing financial interests. **Data and materials availability:** All data needed to support the conclusions are available in the paper or the Supplementary Materials. Additional data that support the findings of this study are available from the corresponding author upon request.

Submitted 11 March 2020
Accepted 22 September 2020
Published 21 October 2020
10.1126/scirobotics.abb6938

Citation: B. Chen, H. Yang, B. Song, D. Meng, X. Yan, Y. Li, Y. Wang, P. Hu, T.-H. Ou, M. Barnell, Q. Wu, H. Wang, W. Wu, A memristor-based hybrid analog-digital computing platform for mobile robotics. *Sci. Robot.* **5**, eabb6938 (2020).

Science Robotics

A memristor-based hybrid analog-digital computing platform for mobile robotics

Buyun Chen, Hao Yang, Boxiang Song, Deming Meng, Xiaodong Yan, Yuanrui Li, Yunxiang Wang, Pan Hu, Tse-Hsien Ou, Mark Barnell, Qing Wu, Han Wang, and Wei Wu

Sci. Robot. **5** (47), eabb6938. DOI: 10.1126/scirobotics.abb6938

Science Robotics (ISSN 2470-9476) is published by the American Association for the Advancement of Science. 1200 New York Avenue NW, Washington, DC 20005. The title *Science Robotics* is a registered trademark of AAAS.